A numerical extrapolation method for complex conductivity of disordered metals

S. Kern,[1] P. Neilinger,[1,2] D. Manca,[1] J. Greguš,[1] S. Volkov,[1] and M. Grajcar[1,2]

[1]*Department of Experimental Physics, Comenius University, SK-84248 Bratislava, Slovakia*
[2]*Institute of Physics, Slovak Academy of Sciences, Dúbravská cesta, Bratislava, Slovakia*

Recently, quantum corrections to optical conductivity of disordered metals up to the UV region were observed. Although this increase of conductivity with frequency, also called anti-Drude behaviour, should disappear at the electron collision frequency, such transition has never been observed or described theoretically. Thus, the knowledge of optical conductivity in a wide frequency range is of great interest. It is well known that the extrapolation of complex conductivity is ill-posed - a solution of the analytic continuation problem is not unique for data with finite accuracy. However, we show that assuming physically appropriate properties of the searched function $\sigma(\omega)$, such as: symmetry, smoothness, and asymptotic solution for low and high frequencies, one can significantly restrict the set of solutions. We present a simple numerical method utilizing the radial basis function approximation and simulated annealing, which reasonably extrapolates the optical conductivity from visible frequency range down to far infrared and up to ultraviolet region. Extrapolation obtained on MoC and NbN thin films was checked by transmission measurement across a wide frequency range.

I. INTRODUCTION

Optical properties of thin films, especially superconducting metals are nowadays of great interest. Knowledge of electric response is essential for the rapidly expanding field of superconducting devices e.g. photon detectors,[1] as well as for purely academic purposes due to presence of phenomena like weak localization. Therefore, this class of materials attracts much investigation nowadays.[2–4] Measurement of optical properties in a broad frequency range is often demanding and the experimental window of devices is naturally limited. In such a case, the data are fitted by causally paired model functions to extrapolate the complex conductivity $\sigma(\omega)$. Unfortunately, there is no easily implementable model for the quantum corrections to high frequency conductivity,[5] which are significant in disordered metals. Nevertheless, the Kramers-Kronig relations can be utilized to a certain degree to extrapolate the complex response function from the experimental window to a larger frequency interval.[6]

We present a model-independent determination of $\sigma(\omega)$ extending the experimental window of spectroscopic ellipsometry, making use of DC-sheet resistance measured at finite temperature T.

II. METHOD DESCRIPTION

Let a set of complex values $\{\sigma'_e(\omega_i^e) + i\sigma''_e(\omega_i^e)\}$ be the complex conductivity at discrete frequencies ω_i^e from interval $[\omega_{min}^e, \omega_{max}^e]$ as well as at zero frequency, $\sigma'_e(0) = \sigma_{dc}$, measured at finite temperature T. We start with discretization of the ω - axis. Taking into account that the error of analytical continuation of experimental data measured with finite precision increases exponentially with distance from the known interval,[7] we use a logarithmic scale. This also helps to avoid problems with splining square-root and logarithmic singularities with polynomial functions. We introduce a new discrete variable x_i with values

$$\begin{aligned} x_i =& 0, 1, ... \\ & ...k, \frac{1}{a}\ln(\hbar\omega_0^e/k_BT), \frac{1}{a}\ln(\hbar\omega_1^e/k_BT), ... \\ & ..., \frac{1}{a}\ln(\hbar\omega_N^e/k_BT), l, l+1, ..., n, \end{aligned} \tag{1}$$

where number of points k below experimental window is set by parameter $a = \ln(\hbar\omega_0^e/k_BT)/(k+1)$ and l is the lowest integer greater than $\ln(\hbar\omega_{max}^e/k_BT)$. The discretization is obtained simply by

$$\omega_i = \frac{k_BT}{\hbar} e^{a\cdot x_i}. \tag{2}$$

An example of such procedure is shown in Fig. 1, where the exponential spacing of red points ω_i is interrupted by the experimental values (blue points) at ω^e. Values of the real part of conductivity at the frequencies ω_i are denoted by y_i, i.e. $y_i = \sigma'(\omega_i)$ and they will become the fitting parameters to be optimized. The integer n determining the number of fitted points can be estimated as the index of a reasonably high value of ω_n, where the conductivity can be safely fixed to zero since $\sigma(\omega \to \infty) \to 0$, whereas the contributions from high energy transition, being far enough from the studied region, are included in parameter ϵ_∞ introduced later on. According to Fermi liquid theory, finite temperature can be taken into account by the transformation

$$\omega \mapsto \Omega = \sqrt{\omega^2 + \gamma(T)^2}, \tag{3}$$

where $\gamma(T)$ is of the same order of magnitude as $k_BT/\hbar$, often taken as $\gamma(T) = \pi k_BT/\hbar$ (e.g. Eq. 6.7 in Ref. 5). Equation (3) implies that for $\omega \ll \gamma(T)$ the conductivity $\sigma'(\omega)$ is constant and equals to $\sigma_{dc} = \sigma'(\gamma(T))$. Thus a smooth function $y = f_{\{y_i\}}(x)$ can be constructed by a cubic spline using the Radial Basis Function (RBF) method[8] with two boundary conditions, $y_0 = \sigma_{dc}$ and $y_n = 0$. The spline proceeds in the logarithmic scale,

where the distribution of centres x_i given by equation (1) is equidistant which is optimal for RBF method.[9]

From known trial function f, the complex conductivity is calculated as $\sigma'_{\{y_i\}}(\omega) = f_{\{y_i\}}(x(\omega))$ and $\sigma''_{\{y_i\}}(\omega) = \mathcal{H}[\sigma'_{\{y_i\}}(\omega)]$. Here, $\mathcal{H}[\sigma'_{\{y_i\}}(\omega)]$ is the Hilbert transform of $\sigma'_{\{y_i\}}(\omega)$. The curve $f_{\{y_i\}}(x)$ is found as the best fit of its Hilbert transform $\sigma''_{\{y_i\}}(\omega)$ to experimental set of points $\sigma''_e(\omega_i^e)$ by least-squares method, minimizing the functional

$$\mathcal{F}[\sigma'_{\{y_i\}}(\omega)] = \sum_{\omega_j^e} \left(\sigma''_e(\omega_j^e) - \sigma''_{\{y_i\}}(\omega_j^e)\right)^2 + \sum_{\omega_j^e} \left(\sigma'_e(\omega_j^e) - \sigma'_{\{y_i\}}(\omega_j^e)\right)^2. \quad (4)$$

This approach leads to the following key observation: Suppose, for a moment, that the values of $\sigma'_e(\omega_i^e)$ and $\sigma''_e(\omega_i^e)$ were not obtained by measurement, but they were generated by restriction of the domain of a dimensionless model function $g'(\omega)$ and its Hilbert image $g''(\omega)$, i.e. $\sigma'_e(\omega_i^e) = \sigma_0 g'(\omega_i^e)$ and $\sigma''_e(\omega_i^e) = \sigma_0 g''(\omega_i^e)$. It means, that the solution corresponding to the input data $\sigma'_e(\omega_i^e)$ and $\sigma''_e(\omega_i^e)$ is already known (the whole function $g'(\omega)$). It is clear that the spline of finite number of points $f_{\{y_i\}}(x)$ can not perfectly recover the function, even if $y_i = \sigma_0 g'(\omega_i)$. Slight differences yield small but non-zero values of the functional (4), denoted by $\mathcal{F}_0$. However, applying the corresponding optimization method, one can find curves with even lower value of functional (4), while these curves are significantly different from $g'(\omega)$.

This is interpreted as a practical consequence of an ill-posed nature of the problem and in order to regularize it, we add the assumption that the searched function is slowly varying. This can be confirmed by the fact that the relaxation rate Γ in highly disordered metals has a large value and therefore, their conductivity varies on large scales.[4] Utilization of this requirement is based on the following idea: For the sake of simplicity, let $g'(\omega)$ be the Lorentzian

$$g'(\omega) = \frac{1}{1 + (\omega/\Gamma)^2} \quad (5)$$

shown in Fig. 1 as red dashed line. The choice of input data $\sigma'_e(\omega_i^e)$ and the discretization of the problem are depicted in Fig. 1 as blue and red dots, respectively. Let us investigate different solutions with the value of functional (4) less or equal to the $\mathcal{F}_0$. Such solutions have the following property: for example if the red point at ω_{11} is lifted and the red point at ω_{12} lowered, or vice versa, the deviation of the imaginary conductivity from the Drude one, shown in inset of Fig. 1, changes only very slightly and can even decrease the deviation caused by the spline error. Thus, solutions oscillating around the curve with the least structure can be averaged out in a sufficiently large ensemble of generated curves. The curves with energy (4) lower than $\mathcal{F}_0$ can be found utilizing the simulated annealing technique by repeated

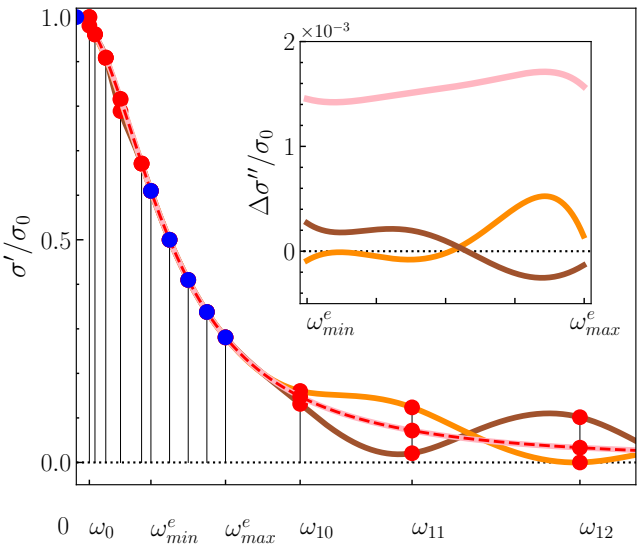

FIG. 1: Reconstruction of Drude complex conductivity by the described method from precisely known values shown as blue points. The real part of Drude conductivity is shown by green dashed line together with three curves which have considerably different values y_i (red points) at higher frequencies. Inset shows the deviation $\Delta\sigma''/\sigma_0 = \mathcal{H}[\sigma'_{\{y_i\}}]/\sigma_0 - g''$ of the imaginary part of conductivity calculated from these curves by Hilbert transform, from Drude one. The deviation is surprisingly larger for pink curve which has all the red points lying on the real part of Drude conductivity than for the brown and orange curves oscillating around it. The values of the functional (4) for pink curve is $\mathcal{F}_0 = 1.2 \times 10^{-5}\sigma_0^2$ and for the orange and brown curves is $2.0 \times 10^{-7}\sigma_0^2$. Nevertheless, the average of brown and orange curves is very close to the Drude one.

melting of the system. We suggest inverse logarithmic temperature decay and rather small step in the form of n-dimensional Gaussian random variable, recommended for continuous optimization.[10] Optimized parameters are forced to be non-negative and the upper bound is chosen high enough to include the shape of an expected solution but not too high to make optimization time-consuming. Points in the measured interval, i.e. values $y_i = \sigma'(\omega_i)$ where $\omega_i \in [\omega^e_{min}, \omega^e_{max}]$ are optimized within intervals $[\sigma'_e(\omega_i^e) - \chi, \sigma'_e(\omega_i^e) + \chi]$, where χ is the noise level of the data.

The generated curves $\sigma'_{\{y_i\}}(\omega)$ which satisfy $\mathcal{F}(\sigma'_{\{y_i\}}(\omega)) \leq \mathcal{F}_0$ are used to compute the averaged curve $\overline{\sigma'}(\omega) = \sigma'_{\{\overline{y_i}\}}(\omega)$. Although the Hilbert transformation is linear, the averaged curve $\overline{\sigma'}(\omega)$ gives a slightly higher value of the functional $\mathcal{F}$. Therefore we search a curve varying similarly as $\overline{\sigma'}(\omega)$ while minimizing the functional (4). Such a multi-objective optimization is performed by the linear scalarization,[11]

i.e. minimizing functional:

$$\tilde{\mathcal{F}}_\lambda[\sigma'_{\{y_i\}}(\omega)] = \mathcal{F}[\sigma'_{\{y_i\}}(\omega)] + \lambda \int_{\omega_0}^{\omega_n} \left(\frac{d^2\sigma'(\omega)}{d\omega^2} - \frac{d^2\overline{\sigma'}(\omega)}{d\omega^2} \right)^2 \mathrm{d}\omega, \tag{6}$$

where ω_0 and ω_n are the first and the last point of the spline defined by equation (2). The parameter λ is not *a priori* known and must be carefully chosen for the particular problem. One can start with a high value of λ, such that $\lambda \gg \mathcal{F}/I$, where I is the integral in (6), estimated with arbitrarily chosen curve from the ensemble. The found solution is very similar to $\overline{\sigma'}(\omega)$ and with a similar value of the first error functional (4). One can lower the value of λ further until the error (4) is lower then $\mathcal{F}_0$. In real data analysis, the precision limit $\mathcal{F}_0$ is set by the measurement error in such a way, that the accepted curve lies within the estimated measurement error.

III. NUMERICAL RESULTS

The extrapolation range and accuracy of the described procedure, i. e. finding reasonable complex conductivity curves to extrapolate the experimental curves with respect to Kramers-Kronig relations, naturally depends on the degree of complexity of the extrapolated functions. Thus, to demonstrate the feasibility of this method, we tested the extrapolation on sets of data created from two functions, which qualitatively describe the real part of the optical conductivity of MoC and NbN thin films, respectively. The conductivity of the former is modelled by a simple function motivated by Ref. 4, which contains the observed square-root quantum corrections to the optical conductivity of these films:

$$g_1(\omega, T) = e^{-\Omega^2/\Gamma_1^2} + Q(\sqrt{\Omega/\Gamma_1} - 1)e^{-4\Omega^2/\Gamma_1^2}. \tag{7}$$

Here, Ω is defined by equation (3), Γ_1 is the scattering rate and the quantumness Q characterizes the strength of the square-root corrections, which are significant up to a certain crossover frequency, chosen to be half of the scattering rate. This function is shown as a red dashed line in square-root-scale in top plot of Fig. 2(a) for $Q = 0.66$. The input data - depicted as blue dots - were obtained by sampling the above function (7) at 20 regularly placed frequencies. Points of the discretization are depicted as red dots. Next, to test the extrapolation of a slightly more complex function, we study a model function with two peaks motivated by Refs. 3,4

$$g_2(\omega, T) = \frac{1}{1 + (\Omega/\Gamma_{2,1})^2} + Q(\sqrt{\Omega/\Gamma_{2,1}} - 1)e^{-4\Omega^2/\Gamma_{2,1}^2} + \frac{r_2}{1 + ((\Omega - \Omega_2)/\Gamma_{2,2})^2}, \tag{8}$$

where $\Gamma_{2,1}/2$ is the cut-off for quantum corrections and r_2 is the peak height ratio. The searched function (8) is shown in top plot of Fig. 2(b) as the red dashed line, the

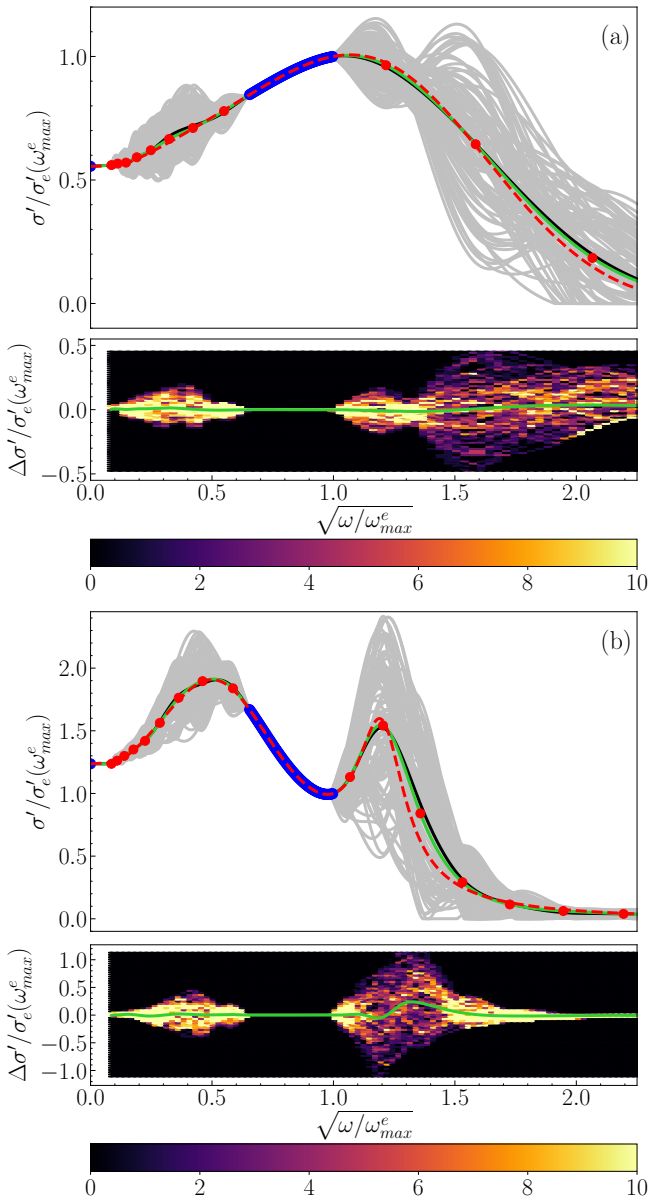

FIG. 2: (a) Top: Red dashed line is a Gaussian model of optical conductivity with square-root quantum corrections (MoC). Blue points laying on the curve are input data for the extrapolation. Silver lines are curves from the ensemble. Black line is a normalized averaged curve $\overline{\sigma'}(\omega) = \sigma'_{\{\overline{y_i}\}}(\omega)$. The final curve is green. Bottom: Histogram showing occupancy of deviations around the searched function by curves from ensemble and deviation of final curve shown as green line. (b) Top: Red dashed line is the optical conductivity as a sum of two Lorentzians with square-root quantum corrections (NbN). Blue points are input data, ensemble curves are silver, the average curve is black and the final curve is green. Bottom: histogram of deviation of curves from ensemble and deviation of final green line.

input data are blue dots and the optimized points are red. A few curves from the averaged ensemble are also shown as silver lines. The average curves are depicted as black lines and the final conductivity is green. As shown in section (IV), function (8) based on Drude-Lorentz model[3] qualitatively describes the measured conductivity of our NbN films, which indicates the presence of two peaks in optical conductivity.

The results presented in Fig. 2 show the usability of the procedure. For the $g_1(\omega)$ curve, there is good agreement of final green curve with the original curve (7) at both higher and lower frequencies. The deviation $\Delta\sigma' = g_1 - \sigma'_{y_i}$ shown in bottom plot of Fig. 2(a) is below 5%. Shown is also a histogram generated by ensemble of found curves. The conductivity model $g_2(\omega)$ is more complex, therefore the function (8) is accurately reconstructed in the vicinity of the extrapolated region, whereas further from this region the deviation increases. The deviation of final curve from searched function (8) shown in bottom plot of Fig. 2(a) reaches 20% and variance of curves is also larger than for simpler model (7). This is visible at higher frequencies in the slightly underestimated second peak's height, whereas at low frequencies, the function is recovered with lower deviation.

IV. EXTRAPOLATION OF EXPERIMENTAL DATA

The procedure was applied to extrapolate the conductivity of disordered thin films as shown in Fig. 3(a) for MoC and Fig. 3(b) for NbN, respectively. For the details of sample preparation, see supplementary information and Refs. 4,12. Complex conductivity was determined from spectroscopic ellipsometry and DC-conductivity was measured by the Van der Pauw method. The contribution of interband transitions at higher energies must be taken into account in the imaginary part of the conductivity. Following the KK relations, the contribution from the bound electrons can be expressed as $\sigma''_{bound} = -\epsilon_0(\epsilon_\infty - 1)\omega$, where ϵ_0 is the permittivity of vacuum and ϵ_∞ is the bound-electron contribution to the static dielectric constant. For MoC, the value of ϵ_∞ was estimated as 1.4 in Ref. 4 and for NbN we calculated $\epsilon_\infty = 2.6$ utilizing the same procedure, while similar value was estimated in Ref. 3. Subsequently, the corresponding contribution to the imaginary part of the conductivity σ''_{bound} was subtracted from measured data. For MoC conductivity, the extrapolation fits between two theoretical curves, a Lorentzian (red) and a Gaussian (pink), proposed in Ref. 4. Taking $\gamma(T)$ in the form $\pi k_B T/\hbar$ (same as in Ref. 4), the inverse transformation given by the equation (3) allows to compare the extrapolation (dotted lines) with the terahertz-frequency real part of conductivity (light blue thick lines) obtained from the temperature dependent DC transport measurement. The agreement for MoC is very good, especially taking into account the large distance between optical frequencies (500 THz) and the frequency ($\pi kT/h \approx 50$ THz) relevant for transport measurements. The agreement for NbN is less satisfying. However, even for this more complicated conductivity spectra the extrapolation can match the transport measurements reasonably.

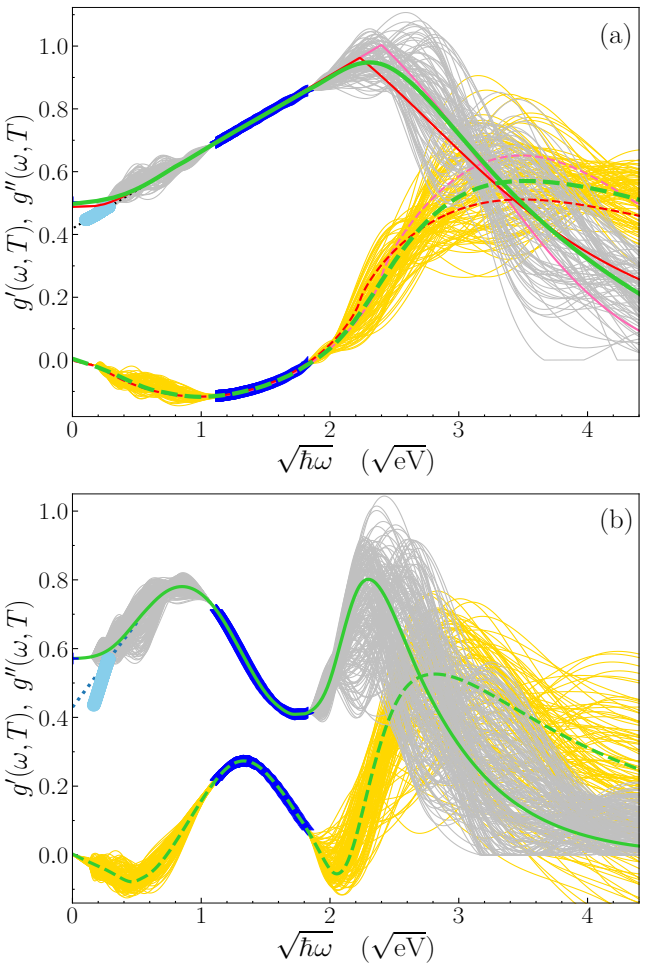

FIG. 3: Real (solid green line) and imaginary (dashed green line) parts of the result of extrapolation applied to the normalized complex sheet conductance $g = g' + ig'' = (\sigma' + i\sigma'')dZ_0$ obtained from spectroscopic ellipsometry (blue data) for MoC (a) and NbN (b) thin films with thicknesses $d = 5$ nm and 3.5 nm, respectively, measured at room temperature. All found complex conductivities with functional (4) $\leq \mathcal{F}_0$ are shown as silver (real part) and gold lines (imaginary part). Since Eq. (3) implies $g'(\omega = 0, T) = g'(\omega = \pi k_B T, 0)$, the real part of complex conductivity at zero temperature (dotted line) obtained from extrapolation procedure can be compared to temperature-dependent DC transport measurement shown as light blue thick lines. Plot (a) also shows two theoretical curves, a Lorentzian (red) and a Gaussian (pink), proposed in Ref. 4.

In order to verify the extrapolation procedure experimentally, the real part of conductivity determined from the extrapolation of ellipsometric data was compared to the conductivity calculated from the transmission of MoC and NbN films (see Supplementary material) di-

rectly measured in a much wider frequency range accessible by our spectrometer, as shown in Fig. 4. The mismatch in the NbN's transmission above 5.0 eV could be caused by interdiffusion between sapphire and NbN. The transmission of sapphire is nearly frequency independent between 0.3-5.0 eV (inset in Fig. 4 (b)), but above 5.0 eV, the transmission strongly depends on impurities in the sapphire.[13] To verify the reliability of transmission data above 5.0 eV, we used them to compute the real part of conductivity, taking the imaginary part from ellipsometry results for the same sample, and used both as the basis for extrapolating a complex conductivity curve, plotting its real part (Figure 4). Such extrapolation failed if the entire transmission dataset (6.2 eV) was used, indicating that such conductivity violates the Kramers-Kronig relations. By the bisection method, we found the cut-off for which the transmission data still process into valid complex conductivity to be 5.4 eV (dotted line, brown); if a data set with cut-off at 5.0 eV was used, the real part of the generated conductivity (orange) matches that produced from ellipsometry alone (green).

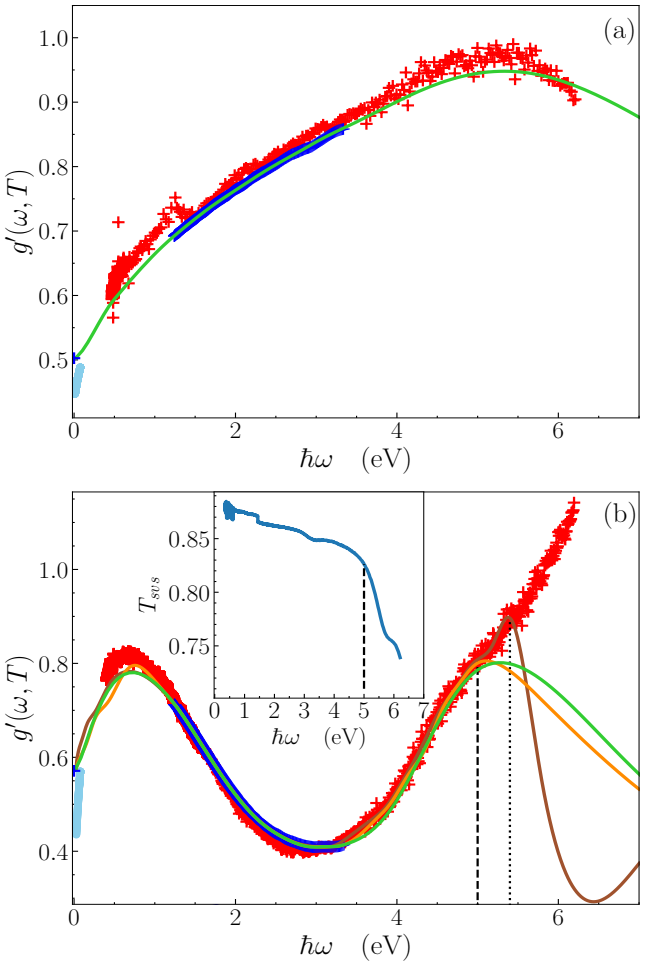

FIG. 4: Green curves are extrapolations of normalized sheet conductance for MoC (a) and NbN (b) obtained from spectroscopic ellipsometry data (blue points) (the same as in Fig. 3) and the experimental values obtained from transport (light blue) and transmission (red) measurements. In plot (b) brown and orange curves are extrapolations of data obtained from transmission measurement with upper cut-off 5.4 eV and 5.0 eV, respectively. The value 5.4 eV of the energy cut-off (dotted line) is the largest, where the extrapolation can be done. The highest value of the cut-off energy, where the influence of the substrate can be neglected, is 5.0 eV. The rapid change in the black curve above 5.0 eV is probably due to the influence of the substrate, whose transmission changes rapidly above this value, as shown in the inset. Data are shown in linear scale.

V. CONCLUSION

A numerical procedure of extrapolating the complex conductivity of disordered metals based on the Kramers-Kronig relations can be implemented if the requirement of slow variation of the conductivity on an energy scale $\lesssim \Gamma$ is met. A slow variation of $\sigma(\omega)$ is reasonably satisfied in highly disordered metals where experimental data do not indicate rapid changes in the conductivity and the described method offers robust and reliable extrapolation procedure of the measured optical conductivity. The range and precision of the extrapolation depend on the complexity of the function. For the simple single-peak model of conductivity, which is the case of MoC thin films, even the DC transport measurements can be reconstructed from the optical measurements, despite the presence of strong quantum corrections. For the more complex, double-peaked conductivity model, which is the case of NbN films, the reliability range of the extrapolation is decreased. However, the extrapolation still reasonably matches the DC measurements and predicts the second peak.

VI. SUPPLEMENTARY MATERIAL

A. Optical properties calculation

Both the ellipsometry data and the extrapolated conductivity were used to obtain the optical properties of our thin films. The real and imaginary part of the complex refractive index are defined in Ref. 14 as

$$n(\omega) = \sqrt{\frac{1}{2}(\Re\{\epsilon_R(\omega)\} + |\epsilon_R(\omega)|)}$$
$$k(\omega) = \mathrm{sgn}(\omega)\sqrt{\frac{1}{2}(-\Re\{\epsilon_R(\omega)\} + |\epsilon_R(\omega)|)}, \quad (9)$$

where ϵ_R is the (complex) relative permittivity given by $\epsilon_R(\omega) = 1 + i\sigma(\omega)/\omega\epsilon_0$.

The transmission T_{vfs} of a thin film with the complex

refractive index $\tilde{n}(\omega) = n(\omega)+ik(\omega)$, placed upon a semi-infinite substrate with index $\tilde{n}_s = n_s$, i.e. vacuum-film-substrate, whose imaginary part is neglected is[15]

$$T_{vfs} = \Big| \frac{2}{(1+\tilde{n}_s)\cos\phi - i(\tilde{n}_s+\tilde{n}^2)\phi_0 \frac{\sin\phi}{\phi}} e^{-i\phi_0} \Big|^2. \quad (10)$$

Here $\phi = \tilde{n}\frac{\omega}{c}d$ and $\phi_0 = \frac{\omega}{c}d$ are phase shifts in the film and in vacuum of thicknesses d, respectively. The transmission T_{vfsv} through a system with finite substrate thickness is

$$T_{vsfv} = \frac{T_{vfs}T_{sv}}{1 - R_{vfs}R_{sv}}, \quad (11)$$

where $T_{sv} = 4n_s/(1+n_s)^2$ is the transmission of the substrate-vacuum interface and the reflection R is obtained from corresponding transmission simply by $1-T$. Next, the transmission of the vacuum-substrate-vacuum system is

$$T_{vsv} = \frac{T_{sv}^2}{1 - R_{sv}^2}. \quad (12)$$

Finally, the equations (11) and (12) are used to express the transmission of the system vacuum-film-substrate-vacuum normalized to the transmission of the substrate itself as

$$\frac{T_{vfsv}}{T_{vsv}} = \frac{T_{vfs}}{T_{sv}} \frac{1 - R_{vs}^2}{1 - R_{vfs}R_{sv}}, \quad (13)$$

which was also a measured quantity. The right-hand side of equation (13) is a function of complex conductivity marked as $T_n(\sigma', \sigma'')$ and can be utilized to calculate one of it's parts, real or imaginary, from another part and from normalized transmission. Instead of inverting equations (9) - (13) one can simply minimize difference between $T_n(\sigma', \sigma'')$ and measured T_{vfsv}/T_{vsv}, namely

$$\sigma' = \arg\min \Big((T_n(\sigma', \sigma'') - T_{vfsv}/T_{vsv})^2 \Big), \quad (14)$$

what is, in fact, plotted in Fig. 4 as red symbols.

B. Sample preparation

The MoC thin film was prepared by means of reactive magnetron deposition from a Mo target in argon-acetylene atmosphere (both gases used of purity 5.0) on c-cut sapphire wafer heated to 200 degrees Celsius. The flow rates of argon and acetylene were set by flow meters. During deposition, the magnetron current was held constant at 200 mA, corresponding to a deposition rate ≈ 11 nm/min. The deposition time, and thus the thickness, was regulated by means of a programmable shutter control interface with a precision of 1 s. The chamber was evacuated to approximately 5×10^{-5} Pa. For details on the preparation of the MoC films and their characterization see Ref. 16. The sheet resistance of the studied MoC sample with a nominal thickness $d = 5$ nm was $R_\square = 720\Omega$.

The thin NbN film was prepared by the pulsed laser ablation from the Nb-target (purity 99.99 %) in the atmosphere of N_2 with added 1 % H2 (purity of the gas mixture is 5.0). The NbN thin film was deposited on the c-cut sapphire wafer, heated to the 600°C. The used laser fluency of KrF laser of 4.9 Jcm^2 corresponded to the deposition rate of 2.4 nm/min. The vacuum chamber was evacuated to the $2 \cdot 10^6$ Pa before deposition. For more details of the preparation of NbN film and its growing features see.[12]

Acknowledgments

This work was supported by the Slovak Research and Development Agency under the contract APVV-16-0372 and by the QuantERA grant SiUCs, by SAS-MTVS.

[1] P. K. Day, H. G. LeDuc, B. A. Mazin, A. Vayonakis, and J. Zmuidzinas, Nature **425**, 817 (2003).

[2] A. Banerjee, R. M. Heath, D. Morozov, D. Hemakumara, U. Nasti, I. Thayne, and R. H. Hadfield, Optical Materials Express **8**, 2072 (2018).

[3] A. Semenov, B. Günther, U. Böttger, H.-W. Hübers, H. Bartolf, A. Engel, A. Schilling, K. Ilin, M. Siegel, R. Schneider, et al., Physical Review B **80**, 054510 (2009).

[4] P. Neilinger, J. Greguš, D. Manca, B. Grančič, M. Kopčík, P. Szabó, P. Samuely, R. Hlubina, and M. Grajcar, Physical Review B **100**, 241106 (2019).

[5] B. Altshuler and A. Aronov, in *Electron-Electron Interactions in Disordered Systems*, edited by A. Efros and M. Pollak (North Holland, 1985).

[6] A. Dienstfrey and L. Greengard, Inverse Problems **17**, 1307 (2001).

[7] L. N. Trefethen, BIT Numerical Mathematics pp. 1–15 (2020).

[8] N. Dyn and D. Levin, SIAM Journal on Numerical Analysis **20**, 377 (1983).

[9] A. Iske (2000).

[10] J. C. Spall, *Introduction to stochastic search and optimization: estimation, simulation, and control*, vol. 65 (John Wiley & Sons, 2005).

[11] M. T. Emmerich and A. H. Deutz, Natural computing **17**, 585 (2018).

[12] S. Volkov, M. Gregor, T. Roch, L. Satrapinskyy, B. Grančič, T. Fiantok, and A. Plecenik, Journal of Electrical Engineering **70**, 89 (2019).

[13] E. R. Dobrovinskaya, L. A. Lytvynov, and V. Pishchik,

Sapphire: material, manufacturing, applications (Springer Science & Business Media, 2009).
[14] E. Hecht, *Optics-Addison* (Wesley, 2002).
[15] Y. Li and T. F. Heinz, arXiv preprint arXiv:1801.00402 (2018).
[16] M. Trgala, M. Žemlička, P. Neilinger, M. Rehák, M. Leporis, Š. Gaži, J. Greguš, T. Plecenik, T. Roch, E. Dobročka, et al., Applied surface science **312**, 216 (2014).